



ELSEVIER

Contents lists available at ScienceDirect

Journal of Sound and Vibration

journal homepage: www.elsevier.com/locate/jsvi

Natural oscillations of a gas bubble in a liquid-filled cavity located in a viscoelastic medium

Alexander A. Doinikov^{*}, Philippe Marmottant

LIPhy, CNRS/Université Grenoble Alpes, F-38000, Grenoble, France



ARTICLE INFO

Article history:

Received 5 May 2017

Revised 10 January 2018

Accepted 15 January 2018

Available online XXX

Keywords:

Cavitation bubble

Liquid-filled cavity

Resonance frequency

Attenuation coefficient

Viscoelastic solid

Dispersion equation

ABSTRACT

The present study is motivated by cavitation phenomena that occur in the stems of trees. The internal pressure in tree conduits can drop down to significant negative values. This drop gives rise to cavitation bubbles, which undergo high-frequency eigenmodes. The aim of the present study is to determine the parameters of the bubble natural oscillations. To this end, a theory is developed that describes the pulsation of a spherical bubble located at the center of a spherical cavity surrounded by an infinite solid medium. It is assumed that the medium inside the bubble is a gas-vapor mixture, the cavity is filled with a compressible viscous liquid, and the medium surrounding the cavity behaves as a viscoelastic solid. The theoretical solution takes into account the outgoing acoustic wave produced by the bubble pulsation, the incoming wave caused by reflection from the liquid-solid boundary, and the outgoing wave propagating in the solid. A dispersion equation for the calculation of complex wavenumbers of the bubble eigenmodes is derived. Approximate analytical solutions to the dispersion equation are found. Numerical simulations are performed to reveal the effect of different physical parameters on the resonance frequency and the attenuation coefficient of the bubble oscillations.

© 2018 Elsevier Ltd. All rights reserved.

1. Introduction

Most theoretical studies on bubble dynamics consider bubbles in an unbounded liquid or near a plane infinite wall. These studies are very numerous and have a long-standing history. Reviews of results obtained can be found in Refs. [1–8]. There are also studies that consider the bubble motion between two plane infinite walls [9] and between tubular walls such as those of blood vessels [10,11]. Theoretical consideration of cavitation phenomena that occur in fully confined liquids, i.e. in liquids surrounded by solid walls in all directions, has received less attention. Such situations, however, occur quite often in nature and technology. Examples are provided by applications in manifold areas such as geology [12,13], processes in porous media [14–16], tensiometer measurements [17], biology [18–21], etc. It should be also pointed out that this problem is of considerable academic interest because it reveals that the resonance behavior of oscillating bubbles becomes qualitatively different in a confined space.

An interesting example of bubble dynamics in a confined space is provided by cavitation phenomena inside the stems of trees [18,20]. These phenomena have an important effect on tree physiology. Hydrodynamic cavitation is typically triggered by high liquid velocities, which, for example, are generated by propellers, resulting in a transient pressure drop according to Bernoulli's law. In trees, water flows are very slow but strong evaporative stresses make the internal pressure inside tree conduits drop down to significant negative values [22–24]. This effect gives rise to a sudden nucleation of microbubbles, which undergo natural

^{*} Corresponding author.

E-mail address: alexander.doinikov@univ-grenoble-alpes.fr (A.A. Doinikov).

oscillations and produce acoustic emissions, mainly in the ultrasonic range [18].

Recently, an experimental technology has been developed that allows one to create spherical liquid-filled microcavities embedded in a stiff polymer hydrogel [16,25]. In such a microcavity, a high negative pressure can be generated by evaporation of liquid from the gel. As a result, the liquid in the cavity experiences a stretched, metastable state. At pressures of about -20 MPa, spontaneous cavitation arises, which relaxes the tension in the cavity. Using this technology, Vincent et al. [16,17,26] have performed experiments for bubbles under the conditions of full confinement. These experiments demonstrated an order-of-magnitude increase in the frequency of bubble oscillations and a very strong damping of the oscillations in comparison with the case of similar bubbles in an unbounded liquid.

Several theoretical approaches have been proposed for the modeling of bubble dynamics in a fully confined liquid [17,26–29]. Vincent et al. [17,26] have proposed a quasi-static model, based on semi-qualitative considerations, that allows one to evaluate the equilibrium radius reached by the growing bubble and the frequency of the bubble oscillation. This model does not consider wave processes in the liquid and in the solid. Vincent and Marmottant [27] and Wang [28] have derived Rayleigh-Plesset-like equations for the finite-amplitude oscillation of a bubble in a liquid confined in an elastic solid. Both derivations use an approximation that introduces a combined compressibility of the liquid and the solid, assuming that the pressure in the cavity varies in time but is uniform in space. Both approaches do not consider wave processes in the solid. Drysdale et al. [29] have developed a theory that describes the linear oscillation of a bubble in a liquid-filled cavity surrounded by an elastic solid. Their theory takes into account the propagation of acoustic waves in the liquid and in the solid and allows one to calculate the natural frequency and the attenuation coefficient of the bubble. The model of Drysdale et al. [29] assumes that the bubble interior is vacuum and ignores surface tension. Therefore, this model cannot be applied to gas bubbles. For the same reason, this model does not allow recovering results obtained for bubbles in an unbounded liquid, such as the Minnaert formula for the bubble natural frequency [30], when the radius of the cavity tends to infinity.

The purpose of the present study is to generalize the model of Drysdale et al. [29] and thus to bring theory closer to real conditions, as well as to remove the problem with the transition from the case of a confined liquid to the case of an unbounded liquid. To this end, we consider important physical effects that have been neglected in the above-mentioned model, namely, the presence of a gas-vapor mixture inside the bubble and viscous damping in the solid medium.

In the situation under study, cavitation bubbles nucleate very fast and therefore they in fact contain vacuum initially. Then, however, they are quickly filled with ballistic water molecules and water vapor. Eventually, depending on their size, the bubbles are filled with air that diffuses from the surrounding liquid where it is dissolved [3]. It is of importance to understand the impact of the gas content on the dynamics of cavitation bubbles in tree conduits.

Another effect that we incorporate in the model is viscous attenuation of acoustic waves in the solid environment. Indeed, real solids are viscoelastic and experimental measurements show that the viscosity of wood is much higher than that of water [31]. Therefore, it is important to reveal the effect of the viscoelastic behavior of wood on the dynamics of cavitation bubbles in tree conduits. Analysis of this effect is also important for other cases of interest, such as microbubbles in soft biological tissues, where viscosity rather than elasticity is a dominant factor.

2. Theoretical model

To simplify the problem and to make it amenable to analytical consideration, we use spherical geometry and approximate the tree conduit as a spherical cavity. We consider a spherical bubble located at the center of a spherical cavity, as shown in Fig. 1. We assume that the cavity is filled with a compressible viscous liquid, the medium surrounding the cavity is a viscoelastic solid of the Kelvin-Voigt type, and the medium inside the bubble is a gas-vapor mixture. It is assumed that the bubble undergoes free oscillations in response to a small random perturbation.

2.1. Bubble

We assume that the pressure of the gas-vapor mixture within the bubble obeys the adiabatic law,

$$p_b = (P_g + P_v) \left(\frac{R_b}{R} \right)^{3\gamma}, \quad (1)$$

where p_b is the time-varying pressure within the bubble, P_g and P_v are the equilibrium pressures of the gas and the vapor, respectively, R is the time-varying bubble radius, R_b is the bubble radius at rest, and γ is the specific heat ratio.

In response to a small initial perturbation, a bubble is known to react as a harmonic oscillator. Therefore, we assume that the bubble oscillation is linear and its time dependence is $\exp(-i\omega t)$, where ω is the angular frequency of the free bubble oscillations. Then R can be represented as

$$R = R_b \left(1 + ae^{-i\omega t} \right). \quad (2)$$

Substituting Eq. (2) into Eq. (1) and linearizing the latter, one obtains

$$p_b \approx (P_g + P_v) \left(1 - 3\gamma ae^{-i\omega t} \right) \quad (3)$$

This equation will be used in the boundary conditions below.

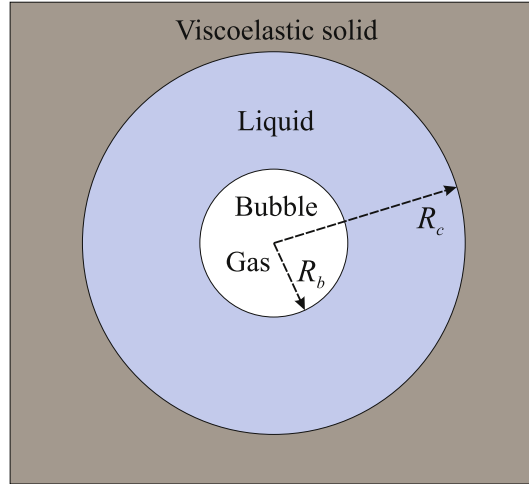


Fig. 1. Geometry of the system under study. A spherical gas bubble is located at the center of a spherical liquid-filled cavity confined in a viscoelastic solid. Three acoustic waves arise in the system: an outgoing wave in the liquid that is generated by the bubble pulsation, an incoming wave in the liquid that is caused by reflection from the liquid-solid interface, and an outgoing wave in the solid that propagates from the liquid-solid interface to infinity.

2.2. Liquid

The linearized equations of motion of a viscous compressible liquid are given by Ref. [32].

$$\rho_0 \frac{\partial \mathbf{v}}{\partial t} = -\nabla p + \eta \nabla^2 \mathbf{v} + \left(\zeta + \frac{1}{3} \eta \right) \nabla (\nabla \cdot \mathbf{v}), \tag{4}$$

$$\frac{\partial \rho}{\partial t} + \rho_0 \nabla \cdot \mathbf{v} = 0, \tag{5}$$

$$p = c^2 \rho, \tag{6}$$

where \mathbf{v} is the liquid velocity, p is the perturbed liquid pressure, η is the shear viscosity, ζ is the bulk viscosity, ρ is the perturbed liquid density, ρ_0 is the liquid density at rest, and c is the speed of sound, which is assumed to be a constant. Eqs. (4)–(6) are the compressible Navier–Stokes equation, the continuity equation, and the equation of state, respectively.

In view of spherical symmetry, the liquid motion is irrotational and hence we can set

$$\mathbf{v} = \nabla \varphi, \tag{7}$$

where φ is the scalar velocity potential. Substitution of Eq. (7) into Eqs. (4)–(6) results in the Helmholtz equation,

$$\nabla^2 \varphi + k^2 \varphi = 0, \tag{8}$$

where the wavenumber k is defined as

$$k = \frac{\omega}{c} \left[1 - \frac{i\omega}{\rho_0 c^2} \left(\zeta + \frac{4}{3} \eta \right) \right]^{-\frac{1}{2}}. \tag{9}$$

A spherically symmetrical solution to Eq. (8) is given by

$$\varphi = \frac{A}{r} e^{i(kr - \omega t)} + \frac{B}{r} e^{-i(kr + \omega t)}, \tag{10}$$

where A and B are constants to be determined by boundary conditions. Eq. (10) describes an outgoing wave produced by the bubble pulsation and an incoming wave that is caused by reflection from the liquid-solid boundary; see Fig. 1. As follows from Eq. (10), the liquid velocity has only the radial component, which is calculated by

$$v = \frac{\partial \varphi}{\partial r} = A \left(\frac{ik}{r} - \frac{1}{r^2} \right) e^{i(kr - \omega t)} - B \left(\frac{ik}{r} + \frac{1}{r^2} \right) e^{-i(kr + \omega t)}. \tag{11}$$

To satisfy the boundary conditions, we also need an expression for the normal stress in the liquid. It is given by Ref. [32].

$$\sigma_{rr} = -p + 2\eta \frac{\partial v}{\partial r} + \left(\zeta - \frac{2}{3} \eta \right) \nabla \cdot \mathbf{v}. \tag{12}$$

The perturbed liquid pressure p is calculated from Eqs. (5), (6) and (8) as

$$p = \frac{i\rho_0 c^2 k^2}{\omega} \varphi. \tag{13}$$

Substituting Eqs. (11) and (13) into Eq. (12) and using Eq. (9), one obtains

$$\sigma_{rr} = -A \left(\frac{i\rho_0 \omega}{r} + \frac{4i\eta k}{r^2} - \frac{4\eta}{r^3} \right) e^{i(kr-\omega t)} - B \left(\frac{i\rho_0 \omega}{r} - \frac{4i\eta k}{r^2} - \frac{4\eta}{r^3} \right) e^{-i(kr+\omega t)}. \tag{14}$$

2.3. Solid

We assume that the medium that surrounds the liquid cavity behaves as a viscoelastic material of the Kelvin-Voigt type. The motion of such a material is governed by the following equation [33]:

$$\rho_s \frac{\partial^2 \mathbf{u}}{\partial t^2} = \mu \nabla^2 \mathbf{u} + (\lambda + \mu) \nabla (\nabla \cdot \mathbf{u}) + \eta_s \nabla^2 \frac{\partial \mathbf{u}}{\partial t} + \left(\zeta_s + \frac{1}{3} \eta_s \right) \nabla \left(\nabla \cdot \frac{\partial \mathbf{u}}{\partial t} \right), \tag{15}$$

where \mathbf{u} is the displacement vector, ρ_s is the density of the solid, λ and μ are the Lamé coefficients, ζ_s is the bulk viscosity, and η_s is the shear viscosity. The spherical symmetry allows one to set

$$\mathbf{u} = \nabla \varphi_s, \tag{16}$$

where φ_s is the scalar potential of the displacement. Substitution of this equation into Eq. (15) yields

$$\nabla^2 \varphi_s + k_s^2 \varphi_s = 0, \tag{17}$$

where the wavenumber k_s is calculated by

$$k_s = \frac{\omega}{c_l} \left[1 - \frac{i\omega}{\rho_s c_l^2} \left(\zeta_s + \frac{4}{3} \eta_s \right) \right]^{-\frac{1}{2}} \tag{18}$$

and c_l denotes the longitudinal wave speed, defined by

$$c_l = \sqrt{\frac{\lambda + 2\mu}{\rho_s}}, \tag{19}$$

A solution to Eq. (17) is written as

$$\varphi_s = \frac{C}{r} e^{i(k_s r - \omega t)}, \tag{20}$$

where C is a constant to be determined. Eq. (20) describes an outgoing wave that propagates from the liquid-solid interface to infinity. The radial component of \mathbf{u} is calculated by

$$u = C \left(\frac{ik_s}{r} - \frac{1}{r^2} \right) e^{i(k_s r - \omega t)}. \tag{21}$$

Finally, the normal stress in a Kelvin-Voigt material is defined by Ref. [33].

$$\tau_{rr} = \lambda \nabla \cdot \mathbf{u} + 2\mu \frac{\partial u}{\partial r} + 2\eta_s \frac{\partial^2 u}{\partial r \partial t} + \left(\zeta_s + \frac{2}{3} \eta_s \right) \nabla \cdot \frac{\partial \mathbf{u}}{\partial t}. \tag{22}$$

Substitution of Eq. (21) into Eq. (22) yields

$$\tau_{rr} = C \left[4(\mu - i\omega\eta_s) \left(\frac{1}{r^3} - \frac{ik_s}{r^2} \right) - \left(\lambda + 2\mu - i\omega\zeta_s - \frac{4i}{3}\omega\eta_s \right) \frac{k_s^2}{r} \right] e^{i(k_s r - \omega t)}. \tag{23}$$

2.4. Boundary conditions

The boundary conditions assume the continuity of velocity and normal stress at the bubble surface and at the liquid-solid interface. These requirements are expressed as follows:

$$v = \frac{dR}{dt} = -i\omega a R_b e^{-i\omega t} \quad \text{at } r = R_b, \tag{24}$$

$$p_b = P_0 + p_{st} - \sigma_{rr} \quad \text{at } r = R_b, \tag{25}$$

$$v = \frac{\partial u}{\partial t} \quad \text{at } r = R_c, \tag{26}$$

$$\sigma_{rr} = \tau_{rr} \quad \text{at } r = R_c, \tag{27}$$

where P_0 is the hydrostatic pressure, R_c is the equilibrium radius of the cavity, and p_{st} is the pressure of surface tension, which is given by

$$p_{st} = \frac{2\sigma}{R} \approx \frac{2\sigma}{R_b} \left(1 - a e^{-i\omega t}\right), \tag{28}$$

with σ denoting the surface tension coefficient.

Eq. (24) allows one to calculate a . Substitution of Eq. (11) into Eq. (24) yields

$$a = \frac{i}{\omega R_b^3} \left[A(ikR_b - 1)e^{ikR_b} - B(ikR_b + 1)e^{-ikR_b} \right]. \tag{29}$$

Substituting Eqs. (3), (11), (14), (21), (23), (28) and (29) into Eqs. (25)–(27), one obtains

$$P_g + P_v = P_0 + \frac{2\sigma}{R_b} \tag{30}$$

and a system of three algebraic equations in the unknowns A , B , and C ,

$$\begin{pmatrix} a_{11} & a_{12} & a_{13} \\ a_{21} & a_{22} & a_{23} \\ a_{31} & a_{32} & a_{33} \end{pmatrix} \times \begin{pmatrix} A \\ B \\ C \end{pmatrix} = 0. \tag{31}$$

The matrix elements a_{nm} are calculated by

$$\begin{aligned} a_{11} &= \left[1 + \left(2\xi_b^2 + \frac{i\omega_b^2}{\omega^2} \right) (i + kR_b) \right] e^{ikR_b} & a_{12} &= \left[1 + \left(2\xi_b^2 + \frac{i\omega_b^2}{\omega^2} \right) (i - kR_b) \right] e^{-ikR_b} \\ a_{13} &= 0 \\ a_{21} &= (ikR_c - 1)e^{ikR_c} & a_{22} &= -(ikR_c + 1)e^{-ikR_c} & a_{23} &= i\omega(ik_s R_c - 1)e^{ik_s R_c} \\ a_{31} &= [1 + 2\xi_c^2(i + kR_c)]e^{ikR_c} & a_{32} &= [1 + 2\xi_c^2(i - kR_c)]e^{-ikR_c} \\ a_{33} &= \frac{i\rho_s\omega}{\rho_0} \left[1 + 2(ik_s R_c - 1) \left(\frac{2}{k_t^2 R_c^2} - i\xi_s^2 \right) \right] e^{ik_s R_c}, \end{aligned} \tag{32}$$

where

$$\omega_b = \frac{1}{R_b} \sqrt{\frac{3\gamma P_0}{\rho_0} + \frac{2(3\gamma - 1)\sigma}{\rho_0 R_b}}, \tag{33}$$

$$\xi_b = \frac{\delta}{R_b}, \quad \xi_c = \frac{\delta}{R_c}, \quad \delta = \sqrt{\frac{2\eta}{\rho_0\omega}}, \tag{34}$$

$$k_t = \frac{\omega}{c_t}, \quad c_t = \sqrt{\frac{\mu}{\rho_s}}, \quad \xi_s = \frac{\delta_s}{R_c}, \quad \delta_s = \sqrt{\frac{2\eta_s}{\rho_s\omega}}. \tag{35}$$

Here, ω_b is the resonance frequency of the bubble in an unbounded perfect liquid [30], δ is the viscous penetration depth in the liquid [32], c_t is the transverse wave speed in the solid [33], and δ_s is the viscous penetration depth in the solid. Note that in most cases of interest, $\xi_{b, c, s} \ll 1$.

2.5. Dispersion equation

The system of Eq. (31) has a nontrivial solution only if its determinant is equal to zero. This condition provides an equation for calculating ω ,

$$\left\{ \left[4 - 2i\xi_s^2 (k_t R_c)^2 \right] (1 - ik_s R_c) - (k_t R_c)^2 \right\} \times \left\{ 1 + \left(2i\xi_b^2 - \frac{\omega_b^2}{\omega^2} \right) (1 + k^2 R_b R_c) - kR_c \cot(kR_c - kR_b) \left[1 + \left(2i\xi_b^2 - \frac{\omega_b^2}{\omega^2} \right) \left(1 - \frac{R_b}{R_c} \right) \right] \right\}$$

$$\begin{aligned}
 & + \frac{\rho_0}{\rho_s} (k_t R_c)^2 (1 - ik_s R_c) \left\{ 1 + 2i\xi_c^2 + \left(2i\xi_b^2 - \frac{\omega_b^2}{\omega^2} \right) [1 + 2i\xi_c^2 (1 + k^2 R_b R_c)] \right. \\
 & \left. - kR_c \cot(kR_c - kR_b) \left[2i\xi_c^2 + \left(2i\xi_b^2 - \frac{\omega_b^2}{\omega^2} \right) \left(2i\xi_c^2 \left(1 - \frac{R_b}{R_c} \right) - \frac{R_b}{R_c} \right) \right] \right\} = 0.
 \end{aligned} \tag{36}$$

Recall that k, k_s and k_t , as well as ξ_b, ξ_c and ξ_s , are functions of ω . In the general case, ω is a complex number whose real part is the resonance frequency and the imaginary part is the attenuation coefficient. Approximate analytical solutions to Eq. (36) are derived in Section 2.6 and exact numerical solutions are considered in Section 3.

It is pertinent to note that in the limit of a rigid solid ($\rho_s \rightarrow \infty$) and negligible viscosity ($\eta, \eta_s \rightarrow 0$), we recover a simpler dispersion equation derived in Ref. [27]: $1 - kR_c \cot(kR_c - kR_b) = 0$.

2.6. Approximate solutions of the dispersion equation

In this subsection, we derive approximate analytical solutions to the dispersion Eq. (36), assuming that $kR_{b,c}, k_{s,t}R_c, \xi_{b,c,s} \ll 1$.

2.6.1. 2nd-order approximation

Let us first expand Eq. (36) up to second order in $kR_{b,c}$ and $k_{s,t}R_c$. Correct to leading viscous terms, the result is a quadratic equation in ω ,

$$\omega^2 + 2i\alpha_0\omega - \omega_0^2 = 0, \tag{37}$$

where

$$\omega_0^2 = \frac{4\mu R_b}{\beta \rho_0 R_c^2 (R_c - R_b)} + \frac{\omega_b^2}{\beta} \left[\frac{R_c}{R_c - R_b} + \frac{4\mu}{3\rho_0 c^2} \left(1 + \frac{R_b}{R_c} + \frac{R_b^2}{R_c^2} \right) \right], \tag{38}$$

$$\beta = 1 + \frac{4\mu}{3\rho_0 c^2} \left(1 - \frac{R_b}{R_c} \right) + \frac{\rho_s R_b}{\rho_0 (R_c - R_b)}, \tag{39}$$

$$\alpha_0 = \frac{2\mu R_b}{\beta \rho_0 c_l R_c (R_c - R_b)} + \frac{2\eta_s R_b}{\beta \rho_0 R_c^2 (R_c - R_b)} + \frac{2\eta}{\beta \rho_0 R_b^2} \left(1 + \frac{4\mu}{3\rho_0 c^2} \right) \left(1 + \frac{R_b}{R_c} + \frac{R_b^2}{R_c^2} \right). \tag{40}$$

A solution to Eq. (37) is given by

$$\omega = -i\alpha_0 + \omega_0 \sqrt{1 - \frac{\alpha_0^2}{\omega_0^2}}. \tag{41}$$

The resonance frequency is defined as $f_r = \text{Re}[\omega]/2\pi$ and the attenuation coefficient is equal to α_0 .

Comparison of Eq. (38) with a similar result obtained by Drysdale et al. [29] for a vacuum bubble shows that the presence of gas inside a bubble leads to a significant difference. Eq. (38) reveals that the resonance frequency of a gas bubble in a solid confinement is determined by two contributions. The first term in Eq. (38) comes from the elastic properties of the confining solid medium, while the second term comes from the gas content of the bubble. This term is absent from the result of Drysdale et al. [29] For $R_c \rightarrow \infty$, the first term in Eq. (38) vanishes and the second term reduces to Eq. (33), which gives the resonance frequency of a bubble in an unbounded liquid [30]. Comparison of the first and the second terms of Eq. (38) allows one to evaluate when each of them plays a dominant role. Assuming for simplicity that R_b is small compared to R_c and the surface tension is negligible, one finds that for $R_b > \bar{R}_b$, where

$$\bar{R}_b = R_c \sqrt[3]{\frac{3\gamma P_0}{4\mu} \left(1 + \frac{4\mu}{3\rho_0 c^2} \right)}, \tag{42}$$

the resonance frequency is dominated by the first term. This means that the resonance behavior of the system is governed by the elastic properties of the confining solid medium rather than the properties of the bubble. On the contrary, bubbles with $R_b < \bar{R}_b$ resonate like bubbles in an unbounded liquid. To put it differently, small bubbles do not “feel” the presence of a confining boundary.

Eq. (40) shows that the attenuation consists of three contributions: radiation damping in the solid (the first term), viscous damping in the solid (the second term), and viscous damping in the liquid (the third term). Eq. (40) allows one to estimate the relative contributions of the viscous damping in the liquid and the combined radiation and viscous damping in the solid. Comparing the terms of this equation, one finds that for $R_b/R_c \ll 1$, the viscous damping in the liquid is dominant if

$$R_b < R_c \sqrt[3]{\frac{\eta}{\eta_s + \mu R_c / c_l} \left(1 + \frac{4\mu}{3\rho_0 c^2} \right)}. \tag{43}$$

To ascertain when the viscous damping in the solid may be dominant, we can compare the first and the second terms in Eq. (40). The comparison shows that the viscous damping is dominant if $\eta_s > \mu R_c / c_l$. Typical values of these parameters for biomimetic wood experiments are $\mu = 0.74$ GPa, $R_c = 100$ μm and $c_l = 2111$ m/s; see Section 3. This means that the viscous damping in the solid may be dominant if $\eta_s > 35$ Pa s. It is shown in Section 3 that a typical value of η_s for wood is 0.43 Pa s. This fact suggests that for cavitation in trees, the solid viscosity appears to give only a small correction to the radiation damping. However there are other cases of interest, such as microbubbles in soft biological tissues. The value of μ in soft biological tissues is of the order of a few kPa, while the value of η_s is of the order of 10 Pa s [34]. In this case, the contribution of viscosity to the damping in the confining medium is decisive; see Section 3.

2.6.2. 3rd-order approximation

Comparison with exact numerical solutions given by Eq. (36) (see Section 3) shows that Eq. (41) provides a satisfactory approximation for the resonance frequency. However, Eq. (40) fails in predicting the attenuation coefficient at intermediate values of the ratio R_b/R_c . To improve the approximate equation for the attenuation coefficient, the compressible terms in Eq. (36) should be kept up to third order in $kR_{b,c}$ and $k_{s,t}R_c$. Doing so, with an accuracy to leading viscous terms, one obtains a cubic equation in ω ,

$$a_1\omega^3 + a_2\omega^2 + a_3\omega + a_4 = 0, \quad (44)$$

where

$$a_1 = -\frac{iR_c}{c_l} \left[1 + \frac{4\mu}{3\rho_0 c^2} \left(1 - \frac{R_b}{R_c} \right) \right], \quad (45)$$

$$a_2 = 1 + \frac{4\mu}{3\rho_0 c^2} \left(1 - \frac{R_b}{R_c} \right) + \frac{\rho_s R_b}{\rho_0 (R_c - R_b)} + \frac{4\eta R_c}{\rho_0 c_l R_b^2} \left(1 + \frac{4\mu}{3\rho_0 c^2} \right) \left(1 + \frac{R_b}{R_c} + \frac{R_b^2}{R_c^2} \right) + \frac{4\eta_s R_b}{\rho_0 c_l R_c (R_c - R_b)}, \quad (46)$$

$$a_3 = \frac{4i}{\rho_0} \left[\frac{\mu R_b}{c_l R_c (R_c - R_b)} + \frac{\eta}{R_b^2} \left(1 + \frac{4\mu}{3\rho_0 c^2} \right) \left(1 + \frac{R_b}{R_c} + \frac{R_b^2}{R_c^2} \right) \right] + \frac{iR_c \omega_b^2}{c_l} \left[\frac{R_c}{R_c - R_b} + \frac{4\mu}{3\rho_0 c^2} \left(1 + \frac{R_b}{R_c} + \frac{R_b^2}{R_c^2} \right) \right] + \frac{4i\eta_s R_b}{\rho_0 R_c^2 (R_c - R_b)}, \quad (47)$$

$$a_4 = -\frac{4\mu R_b}{\rho_0 R_c^2 (R_c - R_b)} - \omega_b^2 \left[\frac{R_c}{R_c - R_b} + \frac{4\mu}{3\rho_0 c^2} \left(1 + \frac{R_b}{R_c} + \frac{R_b^2}{R_c^2} \right) \right]. \quad (48)$$

In the general case, Eq. (44) has three roots. However, calculations show that only one of them has a positive real part, which is necessary to get a physical value for the resonance frequency. This root is calculated by Cardan's formulas as follows:

$$p = \frac{a_3}{a_1} - \frac{a_2^2}{3a_1^2}, \quad (49)$$

$$q = \frac{2a_2^3}{27a_1^3} - \frac{a_2 a_3}{3a_1^2} + \frac{a_4}{a_1}, \quad (50)$$

$$s = \sqrt[3]{-\frac{q}{2} + \sqrt{\left(\frac{p}{3}\right)^3 + \left(\frac{q}{2}\right)^2}}, \quad (51)$$

$$\omega = s - \frac{p}{3s} - \frac{a_2}{3a_1}. \quad (52)$$

The resonance frequency is calculated as $\text{Re}[\omega]/2\pi$ and the attenuation coefficient is equal to $-\text{Im}[\omega]$.

3. Numerical simulations

Simulations were carried out at the following values of the physical parameters: $\rho_0 = 1000$ kg/m³, $c = 1500$ m/s, $\eta = 0.001$ Pa s, $\zeta = 0.003$ Pa s, $\rho_s = 1233$ kg/m³, $\lambda = 4.01$ GPa, $\mu = 0.74$ GPa, $c_l = 2111$ m/s, $c_t = 774.7$ m/s, $\sigma = 0.072$ N/m and $\gamma = 1.4$. These values were chosen to correspond to cavitation experiments on transparent biomimetic wood [27]. To estimate the values of η_s and ζ_s , we have used the results of Vincent [31]. He measured the attenuation of acoustic waves in thin layers of synthetic wood (pHEMA hydrogel) and found that the acoustic intensity I demonstrated a Beer-Lambert type of attenuation. Assuming that the attenuation law is $I = I_0 \exp(-x/l)$, he obtained that the attenuation length $l = 0.7$ mm at 15 MHz in dry synthetic wood. Using this result in Eq. (18) and assuming that $\zeta_s = 3\eta_s$ as is the case with water, we have found $\eta_s = 0.43$ Pa s and $\zeta_s = 1.29$ Pa s.

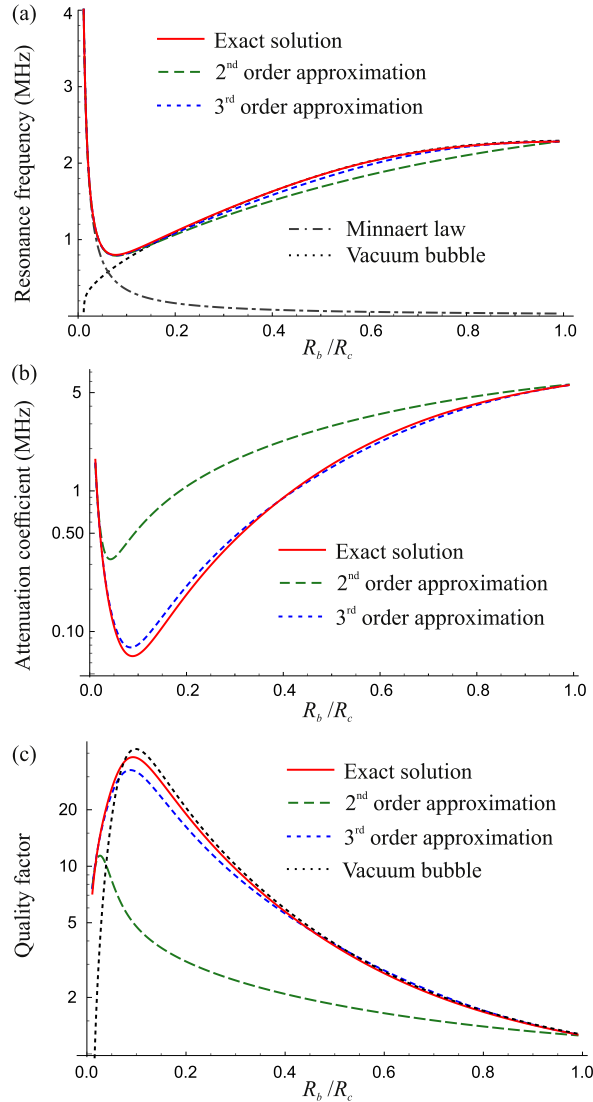


Fig. 2. Comparison of exact numerical solutions calculated by Eq. (36) with approximate analytical solutions calculated by Eqs. (41) and (52). (a) The bubble resonance frequency, (b) the attenuation coefficient of the bubble oscillation and (c) the quality factor of the bubble oscillation are shown as functions of the ratio R_b/R_c . For reference, the results given by the Minnaert law [30] and the theory of Drysdale et al. [29] for a vacuum bubble are also plotted.

Fig. 2 shows the resonance frequency, $f_r = \text{Re}[\omega]/2\pi$, the attenuation coefficient, $\alpha = -\text{Im}[\omega]$, and the quality factor, $Q = \text{Re}[\omega]/2\alpha$, as functions of the ratio R_b/R_c . The plots were obtained at $P_0 = 101.3$ kPa and $R_c = 100$ μm . The solid lines depict the numerical results calculated by Eq. (36), the long-dash lines are given by the 2nd-order approximation, Eq. (41), and the short-dash lines follow from the 3rd-order approximation, Eq. (52). The dash-dot line in Fig. 2(a) shows the resonance frequency given by the Minnaert law, Eq. (33), and the dotted line demonstrates the case that the bubble interior is vacuum [29]. As one can see, the 2nd-order approximation is quite correct for the resonance frequency but fails for the attenuation coefficient. The 3rd-order approximation allows one to achieve a good agreement with the exact numerical results for both the resonance frequency and the attenuation coefficient. Fig. 2(a) shows that at small values of R_b , the resonance frequency follows the Minnaert law and decreases with increasing R_b . However, with increasing R_b/R_c , the presence of the solid environment begins to play a dominant role. As a result, the resonance frequency begins to increase with increasing R_b and tends to the value given by the first term of Eq. (38). Eq. (42) predicts that this change should occur at $R_b/R_c \approx 0.06$. As one can see, the exact numerical solution confirms this prediction. It is also seen that at $R_b/R_c < 0.15$ the curves for a gas bubble and for a vacuum bubble begin to disagree. In this range of bubble radii, the resonance frequency of a gas bubble increases with decreasing R_b , whereas that of a vacuum bubble decreases and eventually ceases to exist because of viscous overdamping, as follows from the results of Drysdale et al. [29]. Fig. 2(b) reveals that the attenuation coefficient passes through a minimum at $R_b/R_c \approx 0.08$. The quality factor has correspondingly a maximum; see Fig. 2(c). Note also that for small bubbles there is a considerable difference between the values

of the quality factor for a gas bubble and a vacuum bubble [29].

It should be mentioned that the values of the resonance frequency given by our theory, shown by the solid curve in Fig. 2(a), are in agreement with the experimental measurements made by Vincent et al. [17,26].

Eqs. (38) and (42) suggest that the presence of the gas inside the bubble, and hence the gas pressure, plays a role only at relatively small values of R_b . With increasing R_b/R_c , when the resonance frequency begins to tend to the value given by the first term of Eq. (38), the effect of the gas inside the bubble becomes insignificant. This prediction is corroborated by Fig. 3, which shows the behavior of the resonance frequency at different values of P_0 , the other parameters being the same as in Fig. 2. Note that the curves in Fig. 3, except the dotted one, were calculated by the exact dispersion equation (36). As one can see, a difference between the curves is observed only when R_b/R_c is smaller than approximately 0.1. At larger values, all the curves tend to the dotted curve given by the theory of Drysdale et al. [29] for a vacuum bubble. Note also that even at small R_b , a noticeable difference between the curves appears only if the change of P_0 is great enough.

Fig. 4 demonstrates the contributions of the liquid viscosity and the solid viscosity to the attenuation coefficient. The curves were calculated by Eq. (36), the parameters being the same as in Fig. 2. The comparison of the solid curve, which depicts the total attenuation coefficient, with the short-dash curve ($\eta_s = 0$) and the long-dash curve ($\eta = 0$) reveals that the contribution of the solid viscosity is insignificant, whereas the contribution of the liquid viscosity is very important at small values of R_b . Its neglect leads to a considerable underestimation of the attenuation coefficient for small bubbles.

Fig. 5 illustrates the dependence of the bubble response on a change in the solid parameters. Fig. 5(a) shows that the resonance frequency increases when the shear modulus μ increases, which is expectable as the rigidity of the system increases. The dependence of the attenuation coefficient on μ , presented in Fig. 5(b), shows that the damping of the bubble oscillations has a maximum at a certain value of μ and its magnitude increases with increasing bubble radius. The behavior of the curves in Fig. 5(b) can be explained using Eq. (40), which gives the attenuation coefficient in the 2nd-order approximation. As was shown above, if the bubble radius is not very small, the main contribution to the damping comes from the radiation loss. This means that the attenuation coefficient is determined by the first term of Eq. (40). Mathematical analysis of this term reveals that it passes through a maximum when, with varying μ , the compression modulus of the solid, $K_s = \rho_s c_s^2$, becomes of the same order as the compression modulus of the liquid, $K_l = \rho_0 c^2$. Also, as one can see directly, the magnitude of this term increases with increasing R_b . Thus, the curves in Fig. 5(b) behave in conformity with the predictions of the first term of Eq. (40). Physically, the

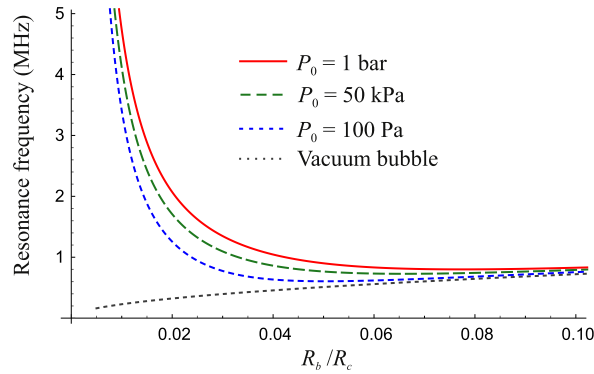


Fig. 3. Behavior of the resonance frequency of the bubble oscillations at different values of the hydrostatic pressure P_0 , the other parameters being the same as in Fig. 2.

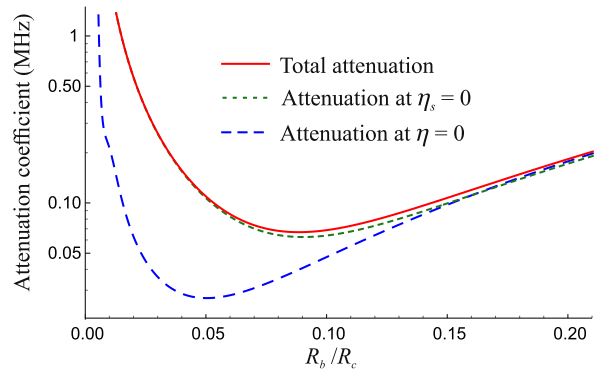


Fig. 4. Comparison of the contributions of the liquid viscosity η and the solid viscosity η_s to the attenuation coefficient of the bubble oscillations. The parameters are as in Fig. 2.

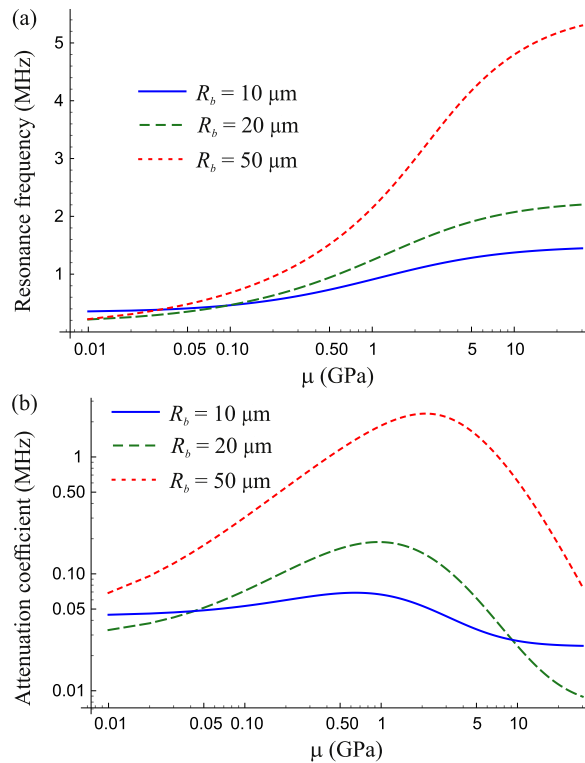


Fig. 5. Dependence of (a) the resonance frequency and (b) the attenuation coefficient on the shear modulus μ at different values of the bubble radius, the other parameters being the same as in Fig. 2.

appearance of the maximum in the attenuation is likely to be caused by the fact that at a certain value of μ , a better acoustic matching between the liquid and the solid is settled so that acoustic energy more easily penetrates through the liquid-solid interface and then is carried away to infinity. Unfortunately, at present there are no experimental data that could be used to verify the predictions of Fig. 5(b).

It was shown above (see Fig. 4) that for the physical parameters characteristic of cavitation experiments on transparent biomimetic wood, the contribution of the solid viscosity η_s to the total damping is insignificant. However there are other cases of interest, such as microbubbles in soft biological tissues. In this case, we have the following typical parameters: Young's modulus $E = 10$ kPa, Poisson's ratio $\nu = 0.495$, $\rho_s = 1000$ kg/m³ and $\eta_s = 10$ Pa s [34]. Converting these elastic parameters to those used in our simulations, we obtain $\mu = 3.34$ kPa, $\lambda = 331$ kPa, $c_t = 1.83$ m/s and $c_l = 18.38$ m/s. The parameters for the liquid and the gas are kept the same as above. Fig. 6 demonstrates the behavior of the attenuation coefficient which is predicted by our theory for the case of soft biological tissues. Compare it with Fig. 4. As one can see, when we set $\eta_s = 0$ in Fig. 6, a great

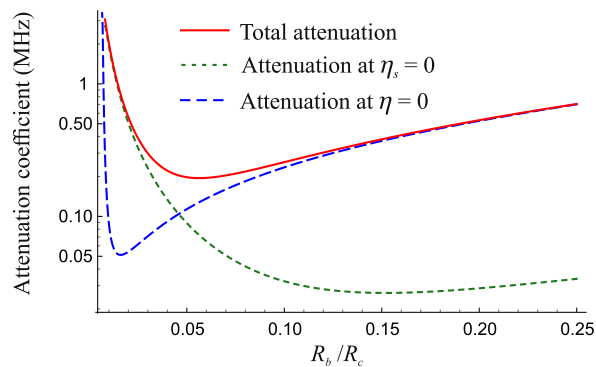


Fig. 6. Comparison of the contributions of the liquid viscosity η and the solid viscosity η_s to the attenuation coefficient of the bubble oscillations. The physical parameters of the confining elastic medium correspond to soft biological tissues [34].

difference from the curve that shows the total attenuation appears, which means that the contribution of η_s cannot be neglected. On the contrary, when we set $\mu = 0$, no difference from the curve of the total attenuation is observed, which means that the contribution of μ is negligible. Thus, in contrast with the damping in wood, it is the viscosity η_s , not the shear modulus μ , that governs the damping in soft biological tissues.

4. Conclusions

The present study develops a theory to describe the behavior of a spherical bubble located at the center of a spherical liquid-filled cavity surrounded by an infinite solid medium. It was assumed that the medium inside the bubble is a gas-vapor mixture, the cavity is filled with a compressible viscous liquid, and the medium surrounding the cavity behaves as a viscoelastic solid. A dispersion equation was derived, whose complex roots allow one to calculate the resonance frequency and the attenuation coefficient of the bubble natural oscillations. Approximate analytical solutions to the dispersion equation were obtained. It was found that the second-order approximation, accurate to second order in compressible terms, predicts quite precisely the resonance frequency but cannot provide correct values for the attenuation coefficient, and hence the quality factor, within the entire range of bubble radii. It was shown that this problem is solved if the accuracy of approximation is increased to third order in compressible terms.

Numerical simulations have been performed at physical parameters characteristic of cavitation experiments on transparent biomimetic wood. It was found that the effect of the gas content inside a bubble on the resonance frequency is insignificant if the bubble radius is comparable to the radius of the cavity as in this case the resonance properties of the system are determined by the elastic properties of the confining solid medium. However, if the bubble radius is relatively small compared to the cavity radius, the gas content plays a key role as in this case the resonance properties of the system are determined by the properties of the bubble.

The contributions of the liquid and solid viscosities to the attenuation coefficient were analyzed. It was found that these contributions are determined by the nature of a confining elastic medium. It was shown that for the physical parameters characteristic of cavitation experiments on transparent biomimetic wood, the attenuation is mainly determined by the radiation loss in the solid, whereas the contribution of the solid viscosity is insignificant and that of the liquid viscosity is important only for small bubbles. However in the case that a confining elastic medium has the properties of soft biological tissue, the role of the viscosity of the confining medium becomes dominant.

Acknowledgement

This research has received funding from the European Research Council under the European Union's Seventh Framework Programme (FP7/2007–2013)/ERC Grant Agreement No. 614655 "Bubbleboost".

References

- [1] M.S. Plesset, A. Prosperetti, Bubble dynamics and cavitation, *Annu. Rev. Fluid Mech.* 9 (1977) 145–185.
- [2] J.R. Blake, D.C. Gibson, Cavitation bubbles near boundaries, *Annu. Rev. Fluid Mech.* 19 (1987) 99–123.
- [3] T.G. Leighton, *The Acoustic Bubble*, Academic Press, San Diego, 1994.
- [4] C.E. Brennen, *Cavitation and Bubble Dynamics*, Oxford University Press, New York, 1995.
- [5] Z.C. Feng, L.G. Leal, Nonlinear bubble dynamics, *Annu. Rev. Fluid Mech.* 29 (1997) 201–243.
- [6] R. Manasseh, A. Ooi, Frequencies of acoustically interacting bubbles, *Bubble Sci. Eng. Technol.* 1 (1–2) (2009) 58–74.
- [7] W. Lauterborn, T. Kurz, Physics of bubble oscillations, *Rep. Prog. Phys.* 73 (2010) 106501.
- [8] J. Rodríguez-Rodríguez, A. Sevilla, C. Martínez-Bazán, J.M. Gordillo, Generation of microbubbles with applications to industry and medicine, *Annu. Rev. Fluid Mech.* 47 (2015) 405–429.
- [9] A.A. Doinikov, A. Bouakaz, Ultrasonically induced dynamics of a contrast agent microbubble between two parallel elastic walls, *Phys. Med. Biol.* 58 (2013) 6797–6814.
- [10] H.N. O-guz, A. Prosperetti, The natural frequency of oscillation of gas bubbles in tubes, *J. Acoust. Soc. Am.* 103 (6) (1998) 3301–3308.
- [11] S. Martynov, E. Stride, N. Saffari, The natural frequencies of microbubble oscillation in elastic vessels, *J. Acoust. Soc. Am.* 126 (6) (2009) 2963–2972.
- [12] E. Roedder, R.J. Bodnar, Geologic pressure determinations from fluid inclusion studies, *Annu. Rev. Earth Planet Sci.* 8 (1980) 263–301.
- [13] D. Marti, Y. Krüger, D. Fleitmann, M. Frenz, J. Rička, The effect of surface tension on liquid-gas equilibria in isochoric systems and its application to fluid inclusions, *Fluid Phase Equil.* 314 (2012) 13–21.
- [14] G.W. Scherer, D.M. Smith, Cavitation during drying of a gel, *J. Non-Cryst. Solids* 189 (1995) 197–211.
- [15] D. Or, M. Tuller, Cavitation during desaturation of porous media under tension, *Water Resour. Res.* 38 (5) (2002) 1061.
- [16] O. Vincent, D.A. Sessoms, E.J. Huber, J. Guioth, A.D. Stroock, Drying by cavitation and poroelastic relaxations in porous media with macroscopic pores connected by nanoscale throats, *Phys. Rev. Lett.* 113 (13) (2014) 134501.
- [17] O. Vincent, P. Marmottant, S.R. Gonzalez-Avila, K. Ando, C.-D. Ohl, The fast dynamics of cavitation bubbles within water confined in elastic solids, *Soft Matter* 10 (10) (2014) 1455–1461.
- [18] M.T. Tyree, M.A. Dixon, Cavitation events in *Thuja occidentalis* L.: Ultrasonic acoustic emissions from the sapwood can be measured, *Plant Physiol.* 72 (4) (1983) 1094–1099.
- [19] M.T. Tyree, J.S. Sperry, Vulnerability of xylem to cavitation and embolism, *Annu. Rev. Plant Physiol. Plant Mol. Biol.* 40 (1989) 19–36.
- [20] H. Cochard, Cavitation in trees, *C. R. Physique* 7 (9–10) (2006) 1018–1026.
- [21] X. Noblin, N.O. Rojas, J. Westbrook, C. Llorens, M. Argentina, J. Dumais, The fern sporangium: a unique catapult, *Science* 335 (2012) 1322.
- [22] A.D. Stroock, V.V. Pagay, M.A. Zwienecki, N.M. Holbrook, The physicochemical hydrodynamics of vascular plants, *Annu. Rev. Fluid Mech.* 46 (1) (2014) 615–642.
- [23] M. Larter, T.J. Brodribb, S. Pfautsch, R. Burlett, H. Cochard, Extreme aridity pushes trees to their physical limits, *Plant Physiol.* 168 (3) (2015) 804–807.
- [24] K.H. Jensen, H. Bruus, N.M. Holbrook, J. Liesche, A. Schulz, M.A. Zwienecki, Sap flow and sugar transport in plants, *Rev. Mod. Phys.* 88 (3) (2016) 1–63.
- [25] T.D. Wheeler, A.D. Stroock, The transpiration of water at negative pressures in a synthetic tree, *Nature* 455 (2008) 208–212.

- [26] O. Vincent, P. Marmottant, P.A. Quinto-Su, C.-D. Ohl, Birth and growth of cavitation bubbles within water under tension confined in a simple synthetic tree, *Phys. Rev. Lett.* 108 (18) (2012) 184502.
- [27] O. Vincent, P. Marmottant, On the statics and dynamics of fully confined bubbles, *J. Fluid Mech.* 827 (2017) 194–224.
- [28] Q.X. Wang, Oscillation of a bubble in a liquid confined in an elastic solid, *Phys. Fluids* 29 (2017) 072101.
- [29] C. Drysdale, A.A. Doinikov, P. Marmottant, Radiation dynamics of a cavitation bubble in a liquid-filled cavity surrounded by an elastic solid, *Phys. Rev. E* 95 (5) (2017) 053104.
- [30] M. Minnaert, On musical air bubbles and the sound of running water, *Philos. Mag. A* 16 (1933) 235–243.
- [31] O. Vincent, Dynamique de bulles de cavitation dans de l'eau micro-confinée sous tension. Application à l'étude de l'embolie dans les arbres (Dynamics of cavitation bubbles in a micro-confined water volume undergoing tension. Application to the study of embolism in trees), PhD thesis, University of Joseph Fourier, Grenoble, 2012. Available from: <http://hal.archives-ouvertes.fr/tel-00807749/>. in French.
- [32] L.D. Landau, E.M. Lifshitz, *Fluid Mechanics*, Pergamon Press, Oxford, 1987.
- [33] L.D. Landau, E.M. Lifshitz, *Theory of Elasticity*, Pergamon Press, Oxford, 1970.
- [34] H. Eskandari, S.E. Salcudean, R. Rohling, J. Ohayon, Viscoelastic characterization of soft tissue from dynamic finite element models, *Phys. Med. Biol.* 53 (2008) 6569–6590.